KSME

Springer

Journal of Mechanical Science and Technology 34 (6) 2020

Original Article
DOI 10.1007/s12206-020-0509-5

Keywords:
· Coefficient of friction
· Force sensor
· Photo-interrupter
· Monolithic flexure
· Tribometry

Correspondence to:
Ismail Lazoglu
ilazoglu@ku.edu.tr

Citation:
Hussain, A., Subasi, O., Lazoglu, I. (2020). A novel sensor using photo-interrupter for measuring static friction coefficient. Journal of Mechanical Science and Technology 34 (6) (2020) 2333~2339. http://doi.org/10.1007/s12206-020-0509-5

Received August 29th, 2019
Revised November 19th, 2019
Accepted April 7th, 2020

† Recommended by Editor Chongdu Cho

A novel sensor using photo-interrupter for measuring static friction coefficient

Abbas Hussain, Omer Subasi and Ismail Lazoglu

Manufacturing and Automation Research Center, Koc University, Istanbul 34450, Turkey

Abstract A force sensor design utilizing a photo-interrupter is presented for measuring the static coefficient of friction (COF). The measurement of ice friction on polymer surfaces, a process that requires detecting forces in the sub-Newton range, is chosen for the study. The photo-interrupter is coupled with a specially designed sensitive flexure, with structural parameters validated through finite element methods, to detect the small forces. The static properties of the sensor are characterized by calibration techniques. An accompanying rotary table is constructed to measure the COF of ice on polymethylmethacrylate (PMMA) and polyester specimens under refrigeration conditions. The experimental results indicate that the device can be utilized to predict the COF. The designed portable and miniature friction measurement setup can be a compact and cost-efficient alternative to bulky tribo-rheometer equipment.

1. Introduction

Determination of the frictional interactions between contacting surfaces is important in virtually all engineering applications; a certain level of friction is mandatory for any kind of motion to take place [1]. The COF is a measured parameter, characterizing the frictional contact between two specimens. In this mechanical interaction, the force perpendicular to the surface is called the normal force (F_n), whereas the force opposing the relative movement is called the tangential friction force (F_t). The ratio of the friction force to the normal force denotes the COF. By generating relative motion between contacting surfaces and measuring the forces, COF can be calculated.

Tribometer is a device commonly used to measure friction forces between two surfaces. Different kinds of tribometers are reported in the literature with differing setups [2, 3]. In tribometers, the friction force is measured using force sensors that provide the feedback to automatized processes. Force sensors utilizing different techniques, including strain gauges [4, 5], piezoelectric sensors [6, 7] and displacement sensors [8], have been a topic of tribometry research. Strain gauges provide a low-cost solution with high linearity but require delicate bonding with the structure. An output voltage amplification circuit is also needed which renders the setup, bulky and data output, noisy [9]. Piezoelectric sensors can measure large stiffness and high natural frequencies, but they suffer from inherent drifts over time due to the leakage of charges in the piezoelectric material [10].

To avoid the disadvantages of piezoelectric sensors and strain gauges, this study employs photo-interrupters, which are optical photo-sensors that detect voltage change depending on the amount of transmitted light in its light-receiving region. The advantages of this small sensor include better accuracy, higher repeatability, low-cost, generation of noiseless signal and elimination of additional amplification electronics. Photo-interrupters have been used in various engineering applications including robotics thanks to their compact dimensions [11-14]. Jeong et al. and Shams et al. both have utilized photo-interrupters for uniaxial force sensing applications in artificial robotic hands [11, 13]. In addition, Subasi et al. developed a photo-interrupter based mini-dynamometer for cutting force measurements in three axes for milling processes [14].

This paper presents a photo-interrupter based force sensor design and an accompanying

rotational table setup for conducting tribology measurements. The developed device is a cost-effective alternative solution to the high-end tribometers used in academia and industry. Additionally, the comparatively small size and portability of the developed system allow conducting friction measurements inside different experimentation compartments, such as refrigeration or pressure-control chambers, where environmental parameters are controlled.

The research on utilizing photo-interrupters paired with monolithic flexures for sub-newton force sensing is still very shallow. This study also demonstrates the possibility of using these compact optical sensors with appropriately designed flexures for sensitive force measurement. Measurement of frictional forces between ice and polymer specimens is specifically chosen as the application of the setup for this study since the forces at play are small-scale in nature. Especially for the aerospace industry, since ice accretion partially depends on the frictional contact between the ice layer and the aviation wing surface, frictional characterization of specially engineered polymer coatings that might alleviate the detrimental icing phenomenon, is crucial [15].

2. Sensor design

2.1 Design requirements

To measure the COF between ice and polymer specimens, the force sensor is designed to measure low friction forces in the sub-newton ranges (0.05 N to 2 N). The previous photo-interrupter based force sensors in the literature were designed to detect forces of higher magnitudes and were implemented along comparably rigid structures. However, to reach a high sensitivity for smaller forces, the pertaining flexure must be designed to be much more pliable. Other critical requirements of the sensor are operability at low temperature (-1.5 °C), reliable accuracy, and repeatability. Testing under dry conditions is designated as the scope of the setup for this study.

2.2 Sensing technique

RPI-131 (ROHM semiconductor, Japan) photo-interrupter is used in this study [16]. It is a slot-type optical sensor (Fig. 1(a)). An LED and a light receiver are coupled by the transmitted light at the two opposite ends of the slot. This creates a light window with a cross-sectional area of 0.7 mm by 0.4 mm. The simple electrical schematic of the photo-interrupter is shown in Fig. 1(b). The voltage reading between the input and output arms of the sensor is dependent on the amount and the intensity of light transferred to the light-receiving end. Thus, the strategy behind using the slotted photo-interrupter is to be able to block the transmitted light in a controlled fashion. With the help of a displacing interrupting shield attached to flexure, the external force that is deforming the flexure can be correlated to the voltage reading of the photo-interrupter.

The load resistance chosen for the sensor is 10 kΩ and with a constant supply of 5 V to the photo-interrupter, 4.80 V is the

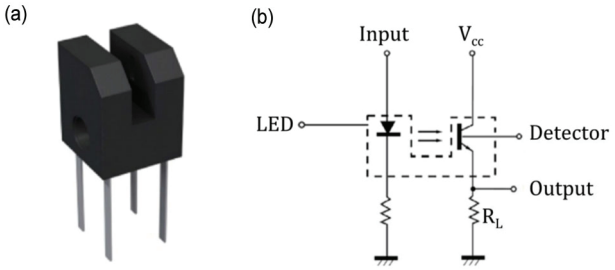

Fig. 1. (a) RPI-131 photo-interrupter; (b) electrical schematic of the photo-interrupter [16].

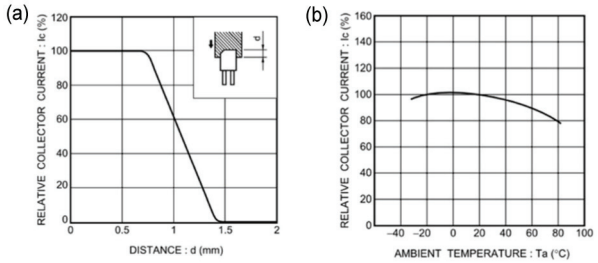

Fig. 2. (a) Relative current change behavior for a displacement of the interrupter shield along the longer dimension of the sensitive light window; (b) relative current change behavior for the operating temperature range [16].

experimentally obtained initial voltage when there is unblocked light transmission. When the light transmission is completely blocked with a shielding member, 0 voltage reading is acquired. The moving shield member is designed in such a way to displace primarily along the 0.7 mm dimension of the window when the external force is applied in the expected direction (Fig. 2(a)). Since the application of the force will be uniaxial and in one direction only, the light window is dedicated to the one-way displacement of the shield. The behavior of the photo-interrupter under its operating temperature range from -25 °C to 85 °C is shown in Fig. 2(b). While at elevated temperatures the relative collector current rapidly drops, it is slightly above 100 % between -10 °C to 0 °C, which is the expected ambient temperature for the experimental setup.

2.3 Sensor working principle

The developed force sensor assembly consists of a deforming flexure, a shielding member, a screw connector and a single photo-interrupter (Fig. 3(a)). The screw connector, while connecting the shield member to the flexure, also acts as the force exertion point. When a force is applied to the end of the screw along its body axis, the flexure will bend accordingly and displace the shield member inside the photo-interrupter's light transmission window (Figs. 3(b) and (c)). Consequently, such a design allows a direct correlation between the force exerted on the screw tip and the voltage change picked up by the sensor. However, as seen in Fig. 3(c), the displacement of the shield member inside the photo-interrupter slot is not purely uniaxial as the midpoint of the member moves both in +X and -Y directions. The displacement in the +X direction is the dominant one

Table 1. Specification of the sensor components.

Flexure thickness	1 mm
Flexure width	4 mm
Flexure length	24 mm
Shielding member thickness	1 mm
Shielding member length	31 mm
Shielding member height	4 mm

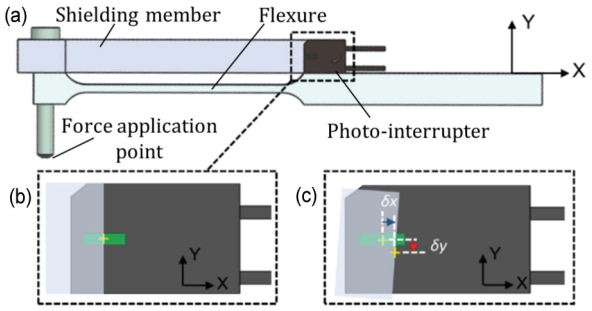

Fig. 3. (a) Force sensor assembly; (b) the initial position of the sensor; (c) displacement of shield inside the light window for bending of the attached flexure.

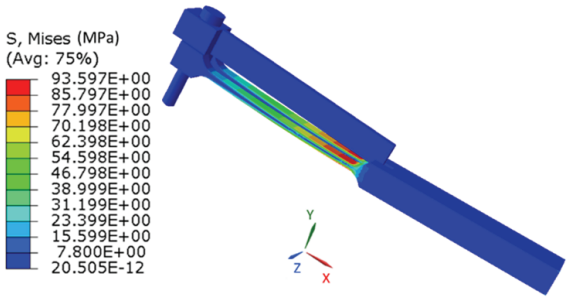

Fig. 4. FEM simulation stress result for 2 N force.

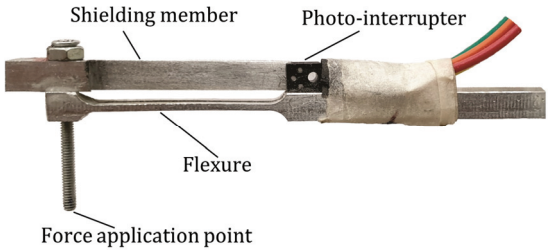

Fig. 5. Manufactured sensor assembly.

and will cause most of the voltage change. While a small tilt angle is created due to the movement of the shield member in the -Y direction, this phenomenon is completely compensated during static calibration of the sensor under various loadings.

3. Finite element analysis

To meet the designated requirement of the sensor, which is having a force range of (0.05 N - 2 N), choosing appropriate dimensional parameters for the flexural component is critical. The thickness of the flexure must be set accordingly to allow the movement of the shielding member in the light transmission window in the X direction for the 2 N force. While it is possible to design a stiff flexure that will allow the sensor to read higher forces, the sensitivity is desired to be maximized in the allowed transmission window length for the relevant small force range. Consequently, to find the appropriate dimensions for the flexure, a numerical static structural study is conducted on a finite element software (ABAQUS 6.14, Dassault Systems).

Initially, a 3D CAD model of the sensor assembly is created (NX v11, Siemens). A straight cantilever beam geometry is chosen for larger displacement and ease of manufacturing of the flexure. The two geometrical parameters that characterize the stiffness of the flexure are the length and thickness. Different parameter combinations are tried until the required displacement for 2 N force on the flexure tip is achieved. The material chosen for the flexure is aluminum 7050 (elastic modulus: 72 GPa), which proved to be sufficiently stiff for the application. For the force simulations, the approximately linear displacement of the shield tip is investigated for the determined force range of the sensor. Table 1 contains the final selected dimensions of the monolithic flexure.

The static structural analysis is conducted using the ABAQUS solver with 104825 nodes and 67851 tetrahedral elements with 0.5 mm sizing. Mesh sensitivity is checked for smaller element sizes, for which no change in the results is observed. Incrementally increasing forces on the sensor tip revealed that until the chosen force ceiling of 2 N, the X-axis displacement of the shield tip follows a linear trend. For the maximum 2 N force applied, Fig. 4(b) portrays that the maximum von Mises stress in the structure is lower than the yielding point of Al7050 (470 MPa) and that no detrimental plastic deformation is expected under loading inside the sensor's operation range.

4. Equipment and calibration

4.1 Equipment

The flexure of the sensor and the shield are manufactured from Al7050 using a Mazak FJV-200 3-axis CNC milling center. The machined components and the photo-interrupter are then assembled such that the end of the shield is placed inside the light transmission window as shown in Fig. 5.

To determine the ice friction coefficient on polymer surfaces, a rotary table mechanism is built, loosely mimicking the standard pin on disk configuration commonly used in literature (Fig. 8). A raised platform is built for the test table and a DC motor is attached to the bottom for the rotation of the platform in a counterclockwise direction. The force sensor is mounted on an attached back wall. Motor control is performed by using the Arduino controller and MATLAB Simulink program. Proportional-integral-derivative (PID) controller is used for motor feedback. The friction force data is acquired using NI-USB-6259 DAQ with 1000 Hz sampling frequency.

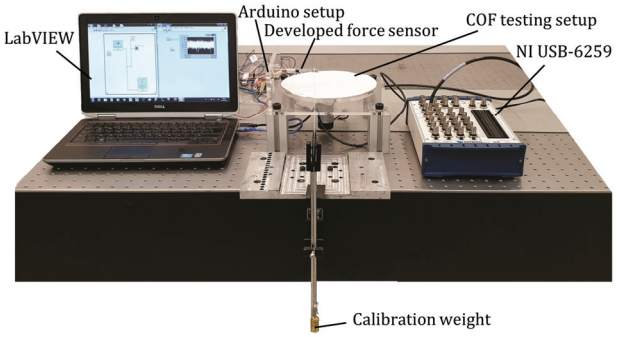

Fig. 6. Static calibration setup of the force sensor.

4.2 Calibration

A calibration setup is prepared to correlate the voltage change data to the loads applied on the sensor, as shown in Fig. 6. Using a pulley system, the sensor is loaded and unloaded with weights and the corresponding voltage output is collected to characterize the voltage response of the sensor. First, the initial voltage is recorded without any loading; the initial value is found as 3.03 V, which reveals that the start position of the shielding member's end tip is approximately at the center of the light transmission window. Fig. 7 shows the sensor output with increasing and decreasing force applied to the sensor.

The calibration curve obtained in Fig. 7 reveals the linearity of the force sensor as the first-order regression model produced a 0.999 goodness of fit parameter (R^2). Thus, the linearity observed in the numerical simulations is also experimentally validated for the chosen range. Eq. (1) shows that the slope of the line, indicating the sensitivity of the manufactured sensor, is 1.421 V per Newton, where F_t is the applied tangential force in Newtons, V_o is the sensor output in Volts and C_o is the offset voltage. The slope is found to be negative because more light is blocked in the photo-interrupter as the force on the tip of the sensor increases, which decreases the voltage.

$$V_o = -1.421F_t + C_o \,. \tag{1}$$

Among other critical static properties of the sensor, hysteresis is checked by incrementally increasing and decreasing the loading (Fig. 7(a)) and repeatability is characterized by loading the sensor 30 times each with 10, 30, 50, 70 and 100 grams (Fig. 7(b)). The resolution, the smallest external force increment that causes a reliably detectable voltage change by the sensor, is found by conducting unit step measurements. The sensor is loaded with 5-gram weight increments up to 100 grams and the step sizes are recorded. The pertaining static calibration characteristics of the sensor are presented in Table 2.

5. Experiments and results

The contacting specimens chosen for the friction measurement experiments are polymer surfaces and ice blocks to imitate the icing of the airplane wing scenario. The polymers are secured to the surface of the rotary table and ice blocks are simply placed stationary on top of the polymer specimen, as shown in Fig. 8. The table is then run at a constant velocity to have the ice block sitting on top of the polymer to engage with the force sensor from the screw tip. After the engagement, the flexure of the sensor bends until the static friction between the polymer and the ice block is overcome and the ice block starts to slide off while the polymer surface continues its motion with the rotating table. The shielding member inside the photo-interrupter moves proportionately and the voltage change data is collected.

The rotary table with the attached force sensor is operated inside a temperature-controlled refrigeration chamber using the

Table 2. Linearity, hysteresis and repeatability errors and resolution of the force sensor.

Linearity error (%)		0.514
Hysteresis error (%)		0.837
Repeatability error (%)	0.1 N	0.316
	0.3 N	0.257
	0.5 N	0.286
	0.7 N	0.465
	1 N	0.444
Resolution (N)		0.050

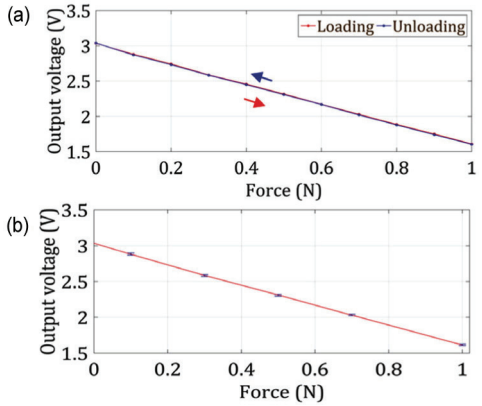

Fig. 7. (a) Calibration curve with hysteresis; (b) repeatability graph for 0.1 N, 0.3 N, 0.5 N, 0.7 N and 1 N.

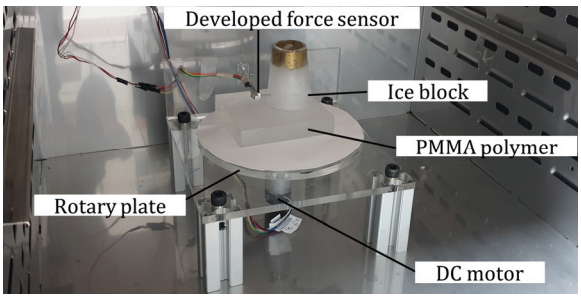

Fig. 8. Experimental setup inside the refrigeration chamber.

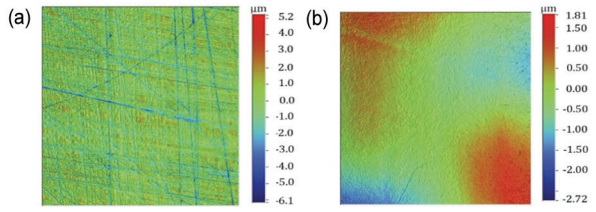

Fig. 9. Surface roughness map obtained via white light interferometer: (a) PMMA polymer; (b) polyester polymer.

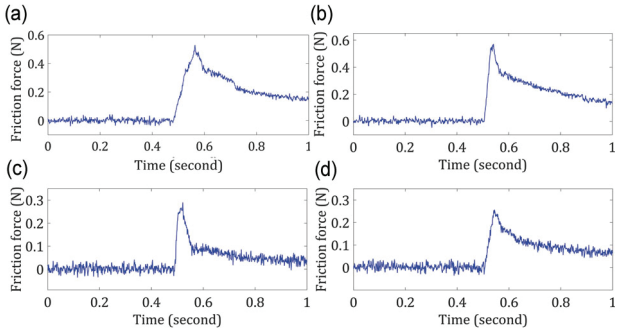

Fig. 10. Measured ice friction force with 3N normal force on PMMA for (a) test 1; (b) test 5, and on polyester for (c) test 1; (d) test 5.

same data acquisition system in Fig. 6. The temperature is maintained at -1.5 ^{o}C inside a laboratory incubator (Pol-Eko Aparatura) and the sliding velocity is kept constant at 0.019 m/s.

5.1 Material preparation

Roughness is a critical parameter that directly affects the magnitude of frictional forces, thus, the surface roughness of each polymer specimen is measured with non-contacting white light interferometry (WLI) measurement system (Bruker Contour GT-K0 3B WLI). Surface maps of PMMA and polyester substrates obtained by the WLI are presented in Fig. 9. The average roughness (Ra) of the PMMA and polyester specimens are found as 641 nm and 442 nm, respectively.

Deionized and distilled water is frozen inside a small fluid container to create the ice specimens that will sit on top of the polymer. Also, to keep roughness as a near-constant parameter throughout the tests, the contacting ice surface is smoothened with fine sandpaper (grit size 400) for a very short period. Since the normal force created solely by the ice would be too small, the normal force is artificially increased by inserting a calibration mass inside the container and having the water freeze with the mass inside. Each ice specimen created this way is weighed with a sensitive balance and the exerted normal force is equalized at 3 N normal force for all ice specimens.

5.2 Results

The measured friction forces with the sensor for two chosen tests with PMMA and polyester specimens are shown in Fig. 10. The solitary peak obtained in the force-time graph represents the engagement of the ice block with the tip of the developed sensor. The force value rapidly reaches its maximum as the ice block is pushed against the sensor tip up until the point the static frictional force between the ice and polymer base is exceeded. After the ice block starts to slide, the force decreases to a plateau in which only dynamic frictional forces are in play with a lower magnitude. Thus, the maximum value measured by the sensor is used in the COF calculation using Amonton's law:

$$\mu = \frac{F_t}{F_n}. \quad (2)$$

Table 3. Measured friction force and calculated COF for PMMA and polyester specimens for constant 3 N normal force.

PMMA			Polyester		
Test #	F_n (N)	COF (μ)	Test #	F_n (N)	COF (μ)
1	0.53	0.18	1	0.29	0.10
2	0.51	0.17	2	0.33	0.11
3	0.60	0.20	3	0.31	0.10
4	0.52	0.17	4	0.25	0.08
5	0.56	0.19	5	0.26	0.08
6	0.60	0.20	6	0.32	0.11
7	0.53	0.18	7	0.23	0.07
8	0.56	0.19	8	0.32	0.11
9	0.55	0.18	9	0.25	0.08
10	0.60	0.20	10	0.28	0.09
Ave.		0.19	Ave.		0.09
St.Dev.		0.01	St.Dev.		0.01

The measured values of friction force and the calculated COF are reported in Table 3. The average COF found for the polyester specimen is lower than the PMMA sample when every process parameter has been kept constant besides the surface roughness. The polyester specimen surface is found to be smoother according to the WLI measurements and the difference in COF between two polymers can be partially attributed to the difference in polymer roughness. However, COF between two interacting surfaces depends on many other parameters and roughness difference, just by itself, cannot adequately explain the magnitudes of the measured coefficients.

6. Discussion

In this study, the design of a cost-efficient force sensor in the sub-newton range using photo-interrupter, along with an accompanying portable rotary table setup is presented for the measurement of static COF. The sensor is found to have acceptable linearity, repeatability, and hysteresis with negligible errors while having a sufficiently small resolution of 0.05 N.

For the given PMMA and polyester surfaces, ice coefficients

of friction are found as 0.19 ± 0.01 and 0.09 ± 0.01, respectively, under constant ambient temperature and rotation velocity. It must be noted that direct validation and comparison of the measured COF with values from literature is almost impossible since, specifically for ice friction, many parameters influence the process. Ambient temperature, rotation velocity of the test plate, wettability and exact chemical composition of the polymer and surface roughness of both specimens are among the critical parameters that make it difficult to replicate previous studies [17].

Even though the lack of a comprehensive validation of the measured COF is among the limitations of the study, the main goal is to demonstrate the sensitive use of photo-interrupters for sub-Newton force sensing, that has not been discussed prior. The reported ice COF for similar polymeric surfaces under comparable testing conditions in the literature range from 0.05 to 0.2 [18-21], which highlights that the measured values are in the correct magnitude range. Consequently, it is safe to conclude that the proposed setup can function as a cost-effective and simple alternative in conducting tribology measurements.

Acknowledgments

This research was supported by the Koc University Manufacturing and Automation Research Center.

Nomenclature

F_t : Tangential force
F_n : Normal force
μ : Coefficient of friction
V_o : Sensor voltage output
C_o : Sensor offset voltage

References

[1] S. Hsu, C. Ying and F. Zhao, The nature of friction: A critical assessment, *Friction,* 2 (2014) 1-26.
[2] M. K. Ramasubramanian and S. D. Jackson, A sensor for measurement of friction coefficient on moving flexible surfaces, *IEEE Sensors Journal,* 5 (2005) 844-849.
[3] T. L. Schmitz, J. E. Action, J. C. Ziegert and W. G. Sawyer, The difficulty of measuring low friction: Uncertainty analysis for friction coefficient measurements, *Journal of Tribology,* 127 (2005) 673.
[4] N. Fujisawa, N. L. James, R. N. Tarrant, D. R. Mckenzie, J. C. Woodard and M. V. Swain, A novel pin-on-apparatus, *Wear,* 254 (2006) 111-119.
[5] V. Lampaert, F. Al-Bender and J. Swevers, Experimental characterization of dry friction at low velocities on a developed tribometer setup for macroscopic measurements, *Tribology Letters,* 16 (2004) 95-105.
[6] D. Pavković, N. Kranjčević, M. Kostelac, Z. Herold and J. Deur, Normal force control for a pin-on-disk tribometer including active or passive suppression of vertical vibrations, *IEEE International Conference on Control Applications* (2012) 488-493.
[7] M. Hoić, M. Hrgetić and J. Deur, Design of a pin-on-disc-type CNC tribometer including an automotive dry clutch application, *Mechatronics,* 40 (2016) 220-232.
[8] R. Novak and T. Polcar, Tribological analysis of thin films by pin-on-disc: Evaluation of friction and wear measurement uncertainty, *Tribology International,* 74 (2014) 154-163.
[9] D. Vischer and O. Khatib, Design and development of high-performance torque-controlled joints, *IEEE Transactions on Robotics and Automation,* 11 (1995) 537-544.
[10] P. Puangmali, K. Althoefer, L. D. Seneviratne, D. Murphy and P. Dasgupta, State-of-the-art in force and tactile sensing for minimally invasive surgery, *IEEE Sensors Journal,* 8 (2008) 371-380.
[11] S. H. Jeong, H. J. Lee, K.-R. Kim and K.-S. Kim, Design of a miniature force sensor based on photointerrupter for robotic hand, *Sensors and Actuators A: Physical,* 269 (2018) 444-453.
[12] G. M. Gu, Y. K. Shin, J. Son and J. Kim, Design and characterization of a photo-sensor based force measurement unit (FMU), *Sensors and Actuators, A: Physical,* 182 (2012) 49-56.
[13] S . Shams, J. Y. Lee and C. Han, Compact and lightweight optical torque sensor for robots with increased range, *Sensors and Actuators, A: Physical,* 173 (2012) 81-89.
[14] O. Subasi, S. G. Yazgi and I. Lazoglu, A novel triaxial opto-electronic based dynamometer for machining processes, *Sensors and Actuators, A: Physical,* 279 (2018) 168-177.
[15] T. Cebeci and F. Kafyeke, Aircraft Icing, *Annual Review of Fluid Mechanics,* 35 (2002) 11-21.
[16] Mouser Electronics, *RPI-131*, http://www.mouser.com/ds/2/348/rpi-131-210869.pdf (Accessed February 22, 2019).
[17] A. M. Kietzig, S. G. Hatzikiriakos and P. Englezos, Ice friction: The effects of surface roughness, structure, and hydrophobicity, *Journal of Applied Physics,* 106 (2009).
[18] C. Stamboulides, P. Englezos and S. G. Hatzikiriakos, The ice friction of polymeric substrates, *Tribology International,* 55 (2012) 59-67.
[19] C. Stamboulides, Microscopic ice friction of polymeric substrates, *Ph.D. Thesis*, The University of British Columbia (2010).
[20] L. Makkonen and M. Tikanmäki, Modeling the friction of ice, *Cold Regions Science and Technology*, 102 (2014) 84-93.
[21] J. R. Blackford, G. Skouvaklis, M. Purser and V. Koutsos, Friction on ice: Stick and slip, *Faraday Discussions,* 156 (2012) 243-254.

Ismail Lazoglu received his M.S. and Ph.D. degrees both in Mechanical Engineering from Georgia Institute of Technology, Atlanta, USA, in 1992 and 1997, respectively. Since 2012, he is working as a Professor of Mechanical Engineering at Koç University, Istanbul, Turkey.

Abbas Hussein received his B.E. degree in Mechanical Engineering, in 2011, from NED University of Engineering and Technology, Pakistan. He obtained his Ph.D. in Mechanical Engineering from Koc University, Istanbul, Turkey, in 2019.

Omer Subasi received his B.S. degree in Mechanical Engineering from California Institute of Technology, CA, US in 2016. He is pursuing his Ph.D. degree in Biomedical Engineering at Koc University, Istanbul.